IOPscience iopscience.iop.org

Home Search Collections Journals About Contact us My IOPscience

X-ray lithography for micro- and nano-fabrication at ELETTRA for interdisciplinary applications

This article has been downloaded from IOPscience. Please scroll down to see the full text article.

2004 J. Phys.: Condens. Matter 16 S3517

(http://iopscience.iop.org/0953-8984/16/33/013)

View the table of contents for this issue, or go to the journal homepage for more

Download details:
IP Address: 129.252.86.83
The article was downloaded on 27/05/2010 at 17:13

Please note that terms and conditions apply.

INSTITUTE OF PHYSICS PUBLISHING JOURNAL OF PHYSICS: CONDENSED MATTER
J. Phys.: Condens. Matter **16** (2004) S3517–S3535 PII: S0953-8984(04)80208-X

X-ray lithography for micro- and nano-fabrication at ELETTRA for interdisciplinary applications

E Di Fabrizio[1], R Fillipo[1], S Cabrini[1], R Kumar[1,4], F Perennes[2], M Altissimo[1], L Businaro[1], D Cojac[3], L Vaccari[1], M Prasciolu[1] and P Candeloro[1]

[1] LILIT-NNL (National Nanotechnology Laboratory)—Nanolithography Beamline-TASC @ELETTRA Synchrotron Light Source, Istituto Nazionale per la Fisica della Materia, SS 14 Km 163.5, I-34012 Basovizza, Trieste, Italy
[2] ELETTRA Synchrotron Light Source, Area Science Park, SS 14 Km 163.5, 34012 Basovizza, Trieste, Italy
[3] University 'Politechnica' of Bucharest, TEF-Department, Optoelectronics Group, 1–3 Boulevard, Luliu Maniu, Bucharest, Romania

E-mail: kumar@tasc.infm.it

Received 6 May 2004
Published 6 August 2004
Online at stacks.iop.org/JPhysCM/16/S3517
doi:10.1088/0953-8984/16/33/013

Abstract
ELETTRA (http://www.elettra.trieste.it/index.html) is a third generation synchrotron radiation source facility operating at Trieste, Italy, and hosts a wide range of research activities in advanced materials analysis and processing, biology and nano-science at several various beam lines. The energy spectrum of ELETTRA allows x-ray nano-lithography using soft (1.5 keV) and hard x-ray (10 keV) wavelengths. The Laboratory for Interdisciplinary Lithography (LIILIT) was established in 1998 as part of an Italian national initiative on micro- and nano-technology project of INFM and is funded and supported by the Italian National Research Council (CNR), INFM and ELETTRA. LILIT had developed two dedicated lithographic beam lines for soft (1.5 keV) and hard x-ray (10 keV) for micro- and nano-fabrication activities for their applications in engineering, science and bio-medical applications. In this paper, we present a summary of our research activities in micro- and nano-fabrication involving x-ray nanolithography at LILIT's soft and hard x-ray beam lines.

(Some figures in this article are in colour only in the electronic version)

1. Introduction

ELETTRA synchrotron radiation facility is located in Trieste, Italy, and hosts a large number of research activities at its several beam lines in areas of advanced materials analysis and

[4] Author to whom any correspondence should be addressed.

processing, biology and nano-science (for details see http://www.elettra.trieste.it). The Italian *National Institute for Physics of Matter*—INFM (for details see http://www.infm.it)—operates through a wide network comprised of two national laboratories, several research units and R&D centres of excellence at Italian universities and at national research facilities to conduct research in a broad spectrum of disciplines. INFM operates one of its national research laboratories, namely the *Laboratory for Advanced Technology and Nano-Science—TASC* (http://www.tasc.infm.it)—at ELETTRA. In 1998, TASC-INFM commissioned the Laboratory for Interdisciplinary Lithography (LILIT, which is also the name of the first wife of Adam in Hebrew mythology) at the ELETTRA Synchrotron Light Source. The LILIT (http://www.elettra.trieste.it/lilit.html) facility was set up to develop advanced micro- and nano-patterning technologies to foster the advanced research in ULSI semiconductor device manufacturing, micro-photonic, magnetic-information storage, biological research, MEMS and other wide varieties of applications. The LILIT facility operates for a wide range of lithography research and maintains comprehensive state-of-the-art infrastructure comprising advanced lithography tools (E-beam, photolithography, FIB, nano-imprint etc) and many other pieces of processing and characterization equipment. We at LILIT had developed two dedicated lithographic beam lines for soft and hard x-rays for micro- and nano-fabrication activities for their applications in engineering, science and bio-medical applications. Also, we provide student access to our state-of-the-art facilities, research opportunities and training to supplement their university coursework with research work. We are pursuing our research in a wide area of research nano-technology with numerous collaborations with research groups from industry, national laboratories and universities as well with the European and international research community. A major portion of our research activities is covered by numerous sponsored research projects with funding from industry, INFM (in house), local prefecture government and the Italian ministry. Our group is also bidding for several projects on nano-technology and bio-engineering research for funding from the European Union under the European Framework-VI Programme.

2. X-ray nano-fabrication activities at LILIT

X-ray nano-lithography (XNL) is a reliable and simple means for replicating sub-20 nm patterns of arbitrary geometry and is ideally suited for nano-structure research. For several years, we at LILIT have been developing the tools and methodologies based on x-ray nano-lithography on our two dedicated beam lines, namely LILIT, which is devoted to proximity x-ray lithography [1, 2]. Another beam line is developed for deep x-ray lithography [3] and LIGA for 3D patterning research activities. Typically, we make our x-ray mask with e-beam lithography (EBL) and very often also employ a combination of photolithography and XNL to fabricate the mask. From the beginning, our research has been focused on the development of state-of-the-art micro- and nano-patterning capabilities that are compatible with soft materials and for the development of powerful new functional micro- and nano-structures by employing x-ray nanolithography (proximity and DXRL), e-beam lithography and conventional photolithography. We have been developing micro- and nano-analytical devices and nano-tools for examining cells, photonic crystal, optical systems, small machines and many other complex functional structures.

The range of technological opportunities available at the nano-scale with a growing capability for making nano-structures of dimensions smaller than 50 nm in size has opened the opportunity to build a complex technology for molecular scale (referring to this as nano-technology) devices. However, with regard to applications at the molecular level, certain apparent fundamental shortcomings of established lithographic techniques are *resolution*,

which is limited to something like 20–30 nm, *line-edge roughness*, becoming comparable to the resolution, *pattern-placement accuracy*, which in some conventional lithographic methods is *worse than their resolution*, etc. Thus, the development of patterning technologies that provide access below the 50 nm length scale (molecular level) represents one of the greatest and perhaps the most important challenges to the field of nano-technology. Towards this end, our research is now focused in an iterative and deeply collaborative fashion on the further development of emerging patterning tools and synthetic hybrid methods based on existing and emerging patterning and assembly methodologies that are unique and allow fabrication of novel micro- and nano-structures, as well as on

(i) the science and technology of surface template-driven assembly strategies that rely on chemical or biochemical recognition events, and
(ii) the experimental and theoretical study of signal transduction in soft matter nano-structures.

These research studies will provide us with the fundamental knowledge base for the rational design of chemical and biological functional nano-devices with significant advantages (sensitivity, selectivity and cost) over conventional systems that derive from the physical and chemical properties of small structures. This paper is divided into two parts. In the first part, we review our micro- and nano-fabrication activities, where we invariably used x-ray nanolithography (in combination of e-beam lithography) for the fabrication of a large variety of structures and devices, including

- *DOEs (diffractive optical elements) for beam shaping and focusing applications*,
    - *zone plates for soft (few hundred electronvolts) and hard (8–50 keV) x-ray and for neutron focusing*,
    - *objectives for DIC x-ray microscopy*,
- *photonic crystals* and
- *magnetic nano-structure*

beside nano-patterning for many unconventional structures.

In the second part, we review our activities for micro-fabrication *using deep x-ray lithography and LIGA techniques for fabrication of*

- *MEMS and micro-fluidic devices and structure*,
- *novel x-ray optical elements*,
- *astronomical adaptive optics* and
- *microsystems for therapeutic drug delivery and space application*.

3. Diffractive optical elements (DOEs)

Diffractive optical elements (DOEs) influence the wavefield by diffraction (reflected or transmitted) and can be tailored to obtain a desired distribution in *amplitude*, *phase* or *polarization*. DOEs can operate over a wide range of wavelength from extreme ultraviolet (EUV) to x-ray radiation. DOEs for *beam shaping* and *focusing applications* have been the most actively researched topic of our group. In this area, we have developed substantial technical expertise in design, micro- and nano-fabrication and testing of wide variety of *diffractive optical elements* for diverse applications. Among many micro-diffractive optical elements developed in our group are *DOEs with continuous* relief in polymeric material [4], a *DOE-microlens* [5] as an *optical mode converter for photonic applications* (fibre–waveguide coupling) and *DOEs for optical tweezers* [6] and zone plates (ZPs) for x-ray [7] and neutron [15] focusing and for

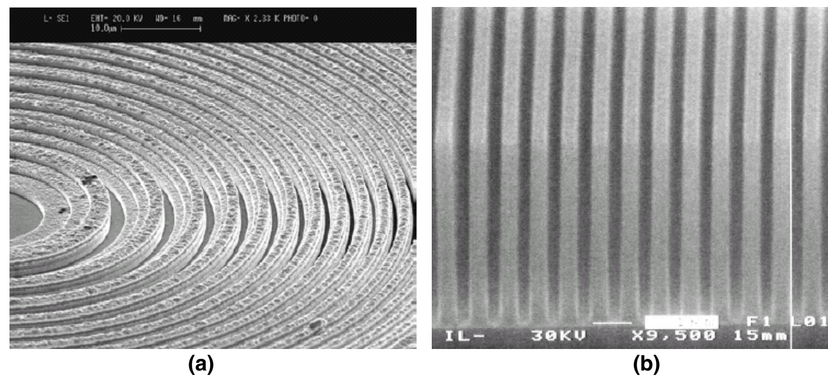

Figure 1. SEM image of (a) fabricated multilevel zone plate in nickel (the experimentally obtained characteristics summary for 8 keV energy is focal length = 1 m, diameter = 150 μm, number of levels $L = 4$ and outermost zone width for the fourth level = 500 nm [7]) and (b) detailing the section of outermost zones in a fabricated ZP for 15–30 keV energy application. The shown feature exhibited an aspect ratio of nearly 15 [12].

differential interference contrast x-ray microscopy [8]. In our brief review, we will cover only our past and recent activities involving ZPs, fabricated primarily for *x-ray* and *neutron focusing applications* by x-ray lithography. In our review we have also included our research work related to *diffractive x-ray optics*, fabricated with EBL but primarily for their end applications in x-ray microscopy and other x-ray optics applications.

3.1. Zone plates for x-rays and neutron focusing

ZPs are diffractive focusing optics elements whose focusing properties have been known for more than 100 years [9]. Zone plates use either phase or amplitude modification to condense an x-ray beam. With amplitude (opaque) zones, theoretically 10% efficiency is possible, while with phase modification efficiency up to as high as 40% can be achieved [7]. Almost all hard x-ray zone plates use a combination of phase and amplitude modification. Zone plates are being used to focus soft x-rays with great success [10]. However, application of ZPs to focus hard x-rays has been limited due to the difficulty in obtaining the required high aspect ratio structure. For ZPs, resolution and efficiency are the most critical parameters. Zone plate resolution is governed by the outermost zone width and the efficiency is determined by the zone thickness i.e. aspect ratio, and demands high resolution patterning. The fabrication of a high aspect ratio ZP was first demonstrated by Bionta *et al* [11] by using a sputtered slice technique. Generally, high efficiency ZPs for-rays focusing are being fabricated with *EBL*. However, the major concern in EBL assisted fabrication is the low yield per electron beam write due to the necessity of proximity corrections for dense micro- and nano-patterning to improve the quality of lithographic structures from the geometrical and resolution points of view. We have addressed this major concern in our research, and accordingly we had perfected a fabrication protocol comprising of EBL for the fabrication of x-ray masks having ZP features, which are then transferred into resist using an x-ray lithography (XRL) process, followed by metal electroplating.

In one of our earliest works on zone plates, Di fabrizio *et al* [7] reported the fabrication of high efficiency, high contrast multi-step (quaternary) Fresnel zone plates (in gold and nickel) as illustrated in figure 1(a) by EBL. These phase zone plates were fabricated and tested for 5–8 keV x-ray energy. Performance evaluations of fabricated zone plates were carried out on

the x-ray microscopy beam line (ID-21) at ESRF (*European Synchrotron Radiation Facility*), which operates over a wide photon energy range of 2–8 keV. The geometrical characteristics of fabricated ZPs at x-ray energy of 8 keV were *focal length* = 1 m; *diameter* = 150 μm; *number of levels* $L = 4$; *outermost zone-width for the fourth level* = 500 nm. The efficiency measurements were performed at 5.5, 6.0, 7.0 and 8 keV energies. At energy of 7 keV, the gold FZP exhibited an efficiency of 38%. However, the highest efficiency of 55% was achieved for the nickel FZP tested at 7 keV. This work was credited as the first experimental demonstration of ZPs in focusing 8 keV x-rays to a 150 nm full width at half maximum (FWHM) focal spot size in the first order focus and an FWHM focal spot size of 90 nm in the third order focus.

In the published work of Alttisimo *et al* [12], we reported fabrication of ZPs using x-ray lithography. Zone plates were fabricated and tested for x-ray energy in the range from 15 to 30 keV and for 25–50 keV. For the ZPs designed fabricated for 25 keV, we obtained 1 mm diameter for the largest zone with outermost zone resolution of 300 nm in 4.5 μm thick nickel (aspect ratio $\sim$ 15) as shown in figure 1(b). ZPs designed and fabricated in gold absorber for 23 keV energy exhibited $\sim$70% efficiency (of the designed theoretical efficiency of 27% for the first diffraction order), a focal length of $f = 8.54$ m and a diffraction limited optical resolution of $\delta_{\mathrm{opt}} = 500$ nm. Another innovative approach which we had developed is the lithographic structure duplication on the backside of the membrane to fabricate a *zone plate doublet*. The schematic concept for the *ZP doublet* and its fabrication process scheme is illustrated in figure 2(a). Using this fabrication approach, we were able to double the effective thickness to fabricate binary pure shift ZPs for hard x-ray focusing in the 60 keV x-ray energy with an efficiency of 35%. In figure 2(b), a portion from a fabricated ZP doublet is shown to demonstrate the reliability of the process in terms of robust process, alignment accuracy and depth of focus. These fabricated ZP doublets have been tested successfully for their application in *differential interference contrast (DIC) application* [13, 14].

New research developments in ZPs are concentrated on testing their application in focusing *neutrons*. Neutrons due to their high penetration are ideally suited in *neutron diffraction* and imaging applications. Ironically, the lack of high efficiency neutron optical elements has been the limitation in realizing neutron focusing devices. In a sense, similar to x-ray focusing using ZPs, *neutron focusing* can also be accomplished by ZPs. To this effect, in 1980 Kearney *et al* [16] first demonstrated the successful use of a *phase reversal ZP* to focus and in imaging a cold neutron beam ($\lambda \approx 20$ Å). However, in contrast to collimated x-ray beams from synchrotrons, a thermal neutron beam as produced by conventional nuclear reactor is much broader ($\sim$few centimetres) in lateral dimension and more inhomogeneous in particle distribution. Thus, inherently a large diameter ZP has to be fabricated in order to intercept a large portion of the neutron beam to maximize the particle flux on the detector. In our recent work [15], we designed, fabricated and tested the ability of ZPs to focus thermal neutron neutrons and our progress is briefly reviewed below.

We fabricated two different kinds of ZP. The first type was a large aperture phase reversal ZP of 5 mm diameter with $f = 400$ nm outermost zone width. The second type of ZP was a 30×30 square matrix on a 1×1 cm^2 surface: i.e. 900 identical ZPs, each having 300 μm diameter and an outermost zone width of 1 μm. Figure 3 shows the micrographs of the fabricated ZP matrix portion, and the central zone of an individual ZP. For both types of ZP, the phase shifter thickness was computed to be around 5 μm to get the maximum efficiency around $\lambda \approx$ a 7 Å. The fabricated ZPs for neutron focusing are shown in figure 3. The ability of these *phase zone plates* (PZPs) in focusing of monochromatic thermal neutrons was tested at the TPA spectrometer located in the *Laboratoire Leon Brillouin*, France. The performances of the 5 mm ZP were measured at $\lambda = 6.85$ Å, with designed parameters: focal length of 3 m and a theoretical efficiency of $\sim$40%. In the experimental set-up (figure 4(a)), a 1 mm pinhole was

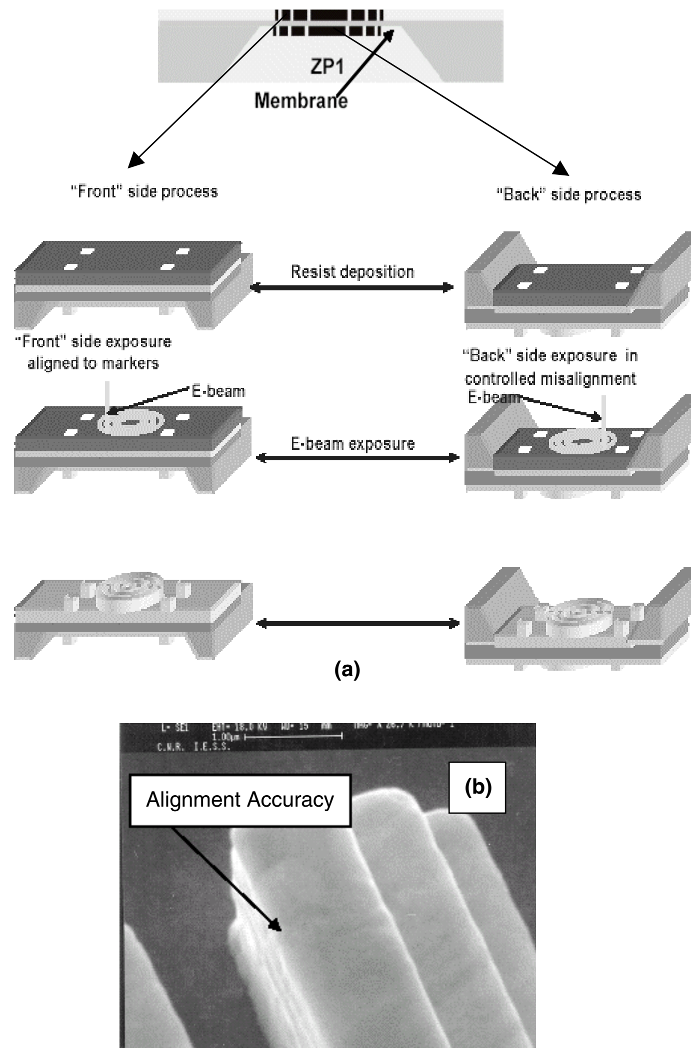

Figure 2. (a) Schematic layout for zone plate doublet for enhancing effective thickness with fabrication process sequence, and (b) SEM image detailing the alignment accuracy achieved in the fabricated ZP doublet.

inserted 3 m upstream of the ZP in order to obtain a parallel beam of 5 mm in diameter at the detector placed 4 m downstream of the lens. The difference between the intensities collected with and without insertion of the ZP is shown in figure 4(a); the focusing effect is clearly visible and the experimentally exhibited efficiency exceeded 20%. The characterization of the ZP matrix was performed at $\lambda = 13.7$ Å, with a 0.8 mm pinhole placed at the image position, 23.6 cm from the lens. In this experimental set-up, without the matrix, the geometrical shadow of the pinhole was expected, whereas a broader spot was formed at the detector position when the matrix was in place, and the intensity map measured on the image plate detector with and without the ZP matrix is shown in figure 4(b). Several experimental problems prevented us from fully characterizing lateral focus dimensions, which include the finite size of the pinhole source, non-homogeneous spatial distribution of the incoming neutron beam, imperfect

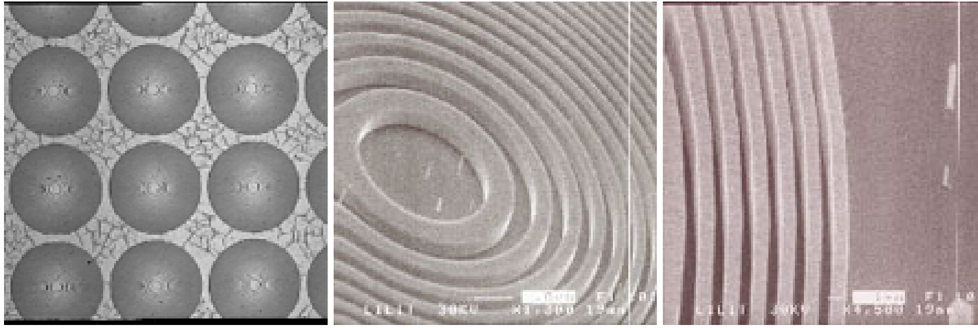

Figure 3. Shown are, from the left, an optical micrograph of a region of a 30 × 30 ZP array for neutron focusing. Each ZP comprises 300 μm diameter, 1 μm outermost zone width in 4.8 μm nickel. In the centre and extreme right frames are shown SEM views of the central zone of an individual ZP and of the outermost zone.

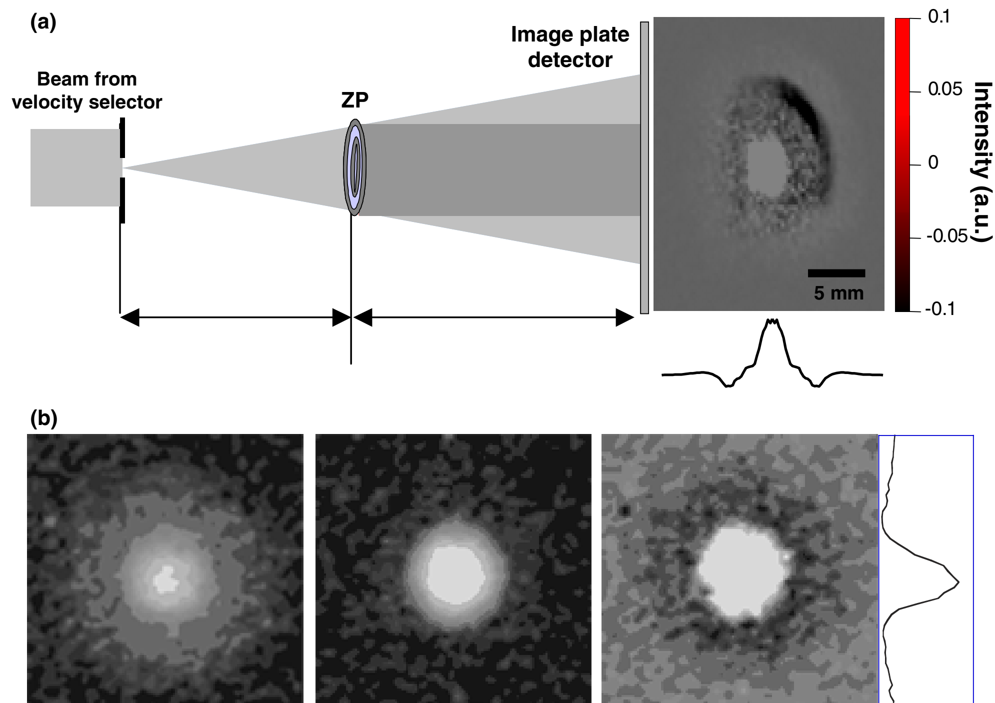

Figure 4. (a) Experimental set-up for testing the 5 mm ZP. The intensity distribution deduced by subtracting the obtained images with and without insertion of the ZP into the beam is also shown at the extreme end. (b) Intensities of the neutron beam obtained with the matrix in the optical path (extreme left), without the matrix, that is, the pinhole image at the detector position (centre), and the difference in intensities with and without the ZP matrix (extreme right picture). It is worth noting that in this measurement what we were seeing was the de-magnified ZP spot at the detector, 4 m away from the pinhole, which in turn was at the focal position [15].

mono-chromaticity of the beam and low spatial resolution of the image plate. Nevertheless, the present results clearly show that a ZP is an excellent choice to focus the neutrons, in

comparison to other optics used in the neutron field. ZPs have the advantage of high efficiency (theoretically ~40%), as demonstrated in our work. This theoretical limit can easily be reached by a more robust fabrication process, since thermal neutrons are not efficiently absorbed by few micron thick layers of low atomic number transition metals. The potential applications that would benefit from the use of ZP optics range from high-resolution neutron imaging to protein crystallography of tiny samples (50–100 μm).

4. Photonic bandgap crystals

Photonic waveguides will be the core element on a photonic integrated circuit (PIC) to guide light from one functional block to the next need to make large bends to keep the light confined. In optical fibre waveguides, light is guided through total internal reflection, and the confinement is accomplished by the contrast in refractive index of the waveguide core and the surrounding cladding. However, it is extremely difficult to create light bending unless the bending radius is comparable to the wavelength. The index contrast between core and cladding is increased by etching the waveguides deeper into the semiconductor substrate. However, as the index contrast increases, the waveguide will support guided modes and can only be corrected by decreasing the *waveguide width*. For very high contrast waveguides, the width becomes so small that it cannot be accurately defined with conventional lithography. To fabricate such ultra-compact waveguides, one must either scale down the *index-guided waveguides*, or alternatively use a *photonic crystal* (PC) slab to guide the light.

Photonic crystals (PCs) are periodic materials which prohibit the propagation of light having frequencies within the so-called bandgap region [17]. When a defect is introduced into a PC, a defect state is created in the PBG, and light can be confined to the defect. By creating a line defect in a photonic crystal, one effectively creates a waveguide, and light has no other option than to follow the defect. Because of this, bends in photonic crystals can, in principle, be very abrupt. Therefore, the most promising application of the PBG structures is to create a novel type of optical waveguide. Perhaps this is the reason that most successful 2D PC structures reported to date utilize some form of *waveguide confinement* [30]. We are involved in the fabrication of 2D and 3D dielectric and metallic bandgap structures [18–29]. In this section, we present our brief review for our research on 2D and 3D PCs.

Our research activity in 2D PCs has mainly been centred on waveguide-embedded 2D PC fabrication and characterization [18–27]. For example, a high index contrast 2D PC slab waveguide [24] in GaAs consisting of a periodic array of holes in a GaAs matrix was fabricated using x-ray lithography. An x-ray mask having triangular and square lattice periods (300–600 nm) with a filling factor (r/a) of 0.3 fabricated by EBL was replicated into resist on SiO_2 (on top of a GaAs substrate) by XRL. Resist patterns were transferred into the SiO_2 layer by RIE and then subsequently transferred to the GaAs layer by successive RIE. The novelty of our design was waveguide slab structures, in which index contrast in cladding layers was obtained. The index contrast in core and cladding layers of the waveguide slab, which was obtained by performing selective wet oxidation (through the holes defined earlier by RIE) of Al-rich AlGaAs in aluminium oxide, and the lower refractive index of the cladding layer was accomplished by removal of aluminium oxide underneath the PC holes by wet chemical etching in order to realize a free standing structure (the bottom cladding layer consists of air) as shown in figure 5(a).

In another similar but different work, we reported 2D photonic crystals fabrication by x-ray lithography and reactive ion etching on an air/GaAs/AlGaAs asymmetric waveguide [18, 21–23]. In this work, in contrast, we exploited *diffraction effects* and *nonlinear response of resists during development* to fabricate a 2D PC with an unconventional unit cell lattice.

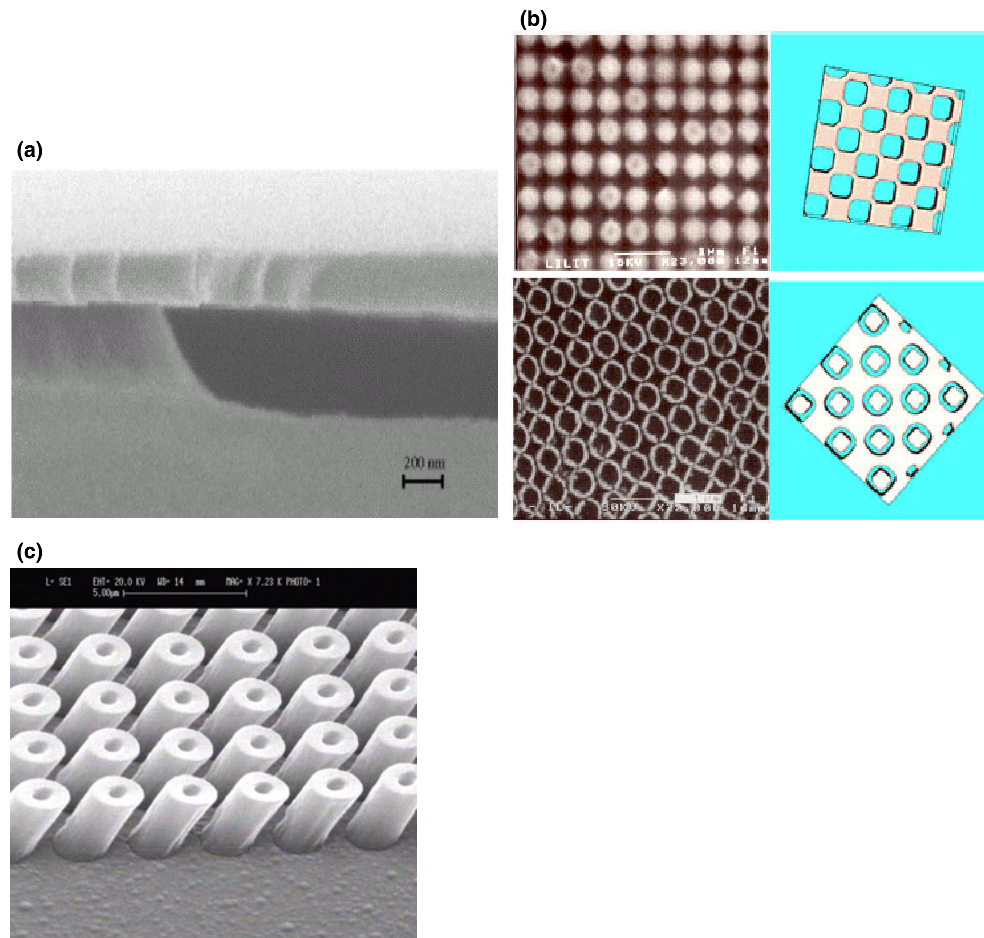

Figure 5. (a) SEM micrograph showing a cross-section of a 2D PC slab waveguide in the GaAs membrane (surrounded on both sides by air). The oxidized region underneath the GaAs waveguide layer was removed by selective wet etching (black region) [26]. (b) SEM micrograph showing 2D PC samples patterned onto air/GaAs/AlGaAs waveguide layers by exploiting x-ray diffraction effects and nonlinear response with a mask–substrate gap of 5 μm (top) and 15 μm (bottom) in resist. Figures adjacent to the SEM micrograph correlate relative x-ray lithography simulations). (c) SEM micrograph showing a 2D PC after dry etching consisting of dielectric rods [24, 25].

Lithographic and other details including optical characterization to demonstrate the accuracy of this fabrication technique are available in [18, 21–23]. The shape of the lattice unit cell was varied by controlling x-ray diffraction effects and nonlinear response of resists during the development process. Rings with or without a central pillar were fabricated with a resolution down to 50 nm. Several theoretical as well experimental studies had clearly established the role of *diffraction* in XRL patterning [30, 31]. In diffraction assisted patterning, to obtain the desired shape and size of the unit lattice cell, *spatial source coherence* and the *mask–substrate gap* are the crucial controlling parameters [31]. For example, with a 5 μm mask–substrate gap, the mask features were very well reproduced. This is the case of *micro-gap* proximity x-ray lithography where a one-to-one replica of the mask feature could be achieved without any appreciable diffraction effects as illustrated in figure 5(b) (top portion). In contrast, the

effects of the diffraction were clearly seen irrespective of the tone of photo-resist [19, 20], when a 15 μm mask–substrate gap was used as shown in figure 5(b) (bottom part). The figures adjacent to the SEM micrograph (figure 5(b)) correlate relative lithography simulations. A fabricated 2D PC after dry etching consisting of dielectric rods is shown in figure 5(c). We also studied the effect of the mask-wafer on the filling factor of the resulting PC. The dielectric fraction on the total unit cell area was very low for negative-tone resist (~9% for 15 μm gap and 28% for 5 μm gap), while for positive-tone (PMMA) resist a filling factor as high 78% was achieved. Although lithography was a critical step, etching submicron arrays of holes is the most crucial task for fabrication of high quality PCs. As practical dimensions for near-infrared applications are in the range $d = 100$–300 nm for hole diameters and $a = 200$–600 nm for the period for mid-infrared ($\lambda =$ could be envisioned with $d = 1$ μm and $a = 2$ μm), or even with pillars instead of holes. We therefore adopted an approach of using membranes over the substrate for PC fabrication. This is because of the limited etch depth ~200–400 nm for the membrane, whereas for the substrate the approach is of the order of ~800 nm in the GaAlAs system around $\lambda = 1$ μm, and shoots up to 2 μm in the InP based system around $\lambda = 1.6$ μm, which suggests an aspect ratio of 6–10 for the substrate approach, instead of 1–2 in the membrane approach. This demand translates into a technological quest for a mask, withstanding the etching process with minimal erosion. The resist itself (e.g. PMMA or any high resolution resist) cannot be used in general. One has to transfer the pattern to another more robust mask of SiO_2 dielectric or preferably metal.

In contrast to their 2D counterparts, 3D PCs [17] have the ability to isolate such a mode by opening a complete bandgap along every direction in 4π steradians. Although these 3D photonic crystals look very promising and have been theoretically widely studied, experimental fabrication of a 3D periodic structure with a complete bandgap embedded with a *defect* or *waveguide* in the bandgap of the PC to provide true guided modes and to have a single mode in the frequency range of interest is still a challenge. The main problem arises because of the sophisticated geometry and intricate arrangement of holes and rods needed to open a gap. Experimentally, Yablonovitch *et al* [17] demonstrated the first complete photonic bandgap structure now known as '*Yablonovite*' or '*three-cylinder*' structure, fabricated by drilling three sets of tilted holes at 35.26° off vertical in a high refractive index material. Since then intensive efforts to transpose these results to the near-infrared range have been researched [28, 29, 32–42] by using a *top-down engineering approach based on microlithography* [33–35, 41, 42], and using a *bottom-up approach* [17, 32], such as *colloidal suspensions* to form *colloidal crystals* or *artificial opals* [17, 32] fabrication of 3D PCs with photonic bandgap at optical wavelength has been reported. Although the technology for fabricating three-dimensional photonic crystals has evolved rapidly in recent years, few methods have been proposed to introduce *defects* at the desired places in photonic crystals. Vlasov *et al* [36], in their work, attempted to create '*defects*' by the infiltration of silicon into *opal lattice agglomerates* and then removing the template by successive chemical etching. Our research on 3D PCs is motivated to address the most difficult to realize 3D PCs and the capability to insert a *waveguide path*. In this section, we review our research activities on 3D PC fabrication and will address our recent breakthrough in the fabrication of *waveguide defects* (WGDs) inside 3D PCs with a newly developed process based on a *two-resist process* [44, 45] which is based on a *combined used of multiple-tilted x-ray lithography* [28, 29] *and e-beam lithography*. In this method that we have developed, and patented, *multiple-tilted x-ray lithography* is used to generate the 3D PC template and e-beam lithography is used to *create a linear defect* of desired shape and dimension in the created lattice.

In multiple-tilted x-ray lithography, during exposure, each opening of the x-ray mask during an exposure will expose the resist along designated directions, generating different holes.

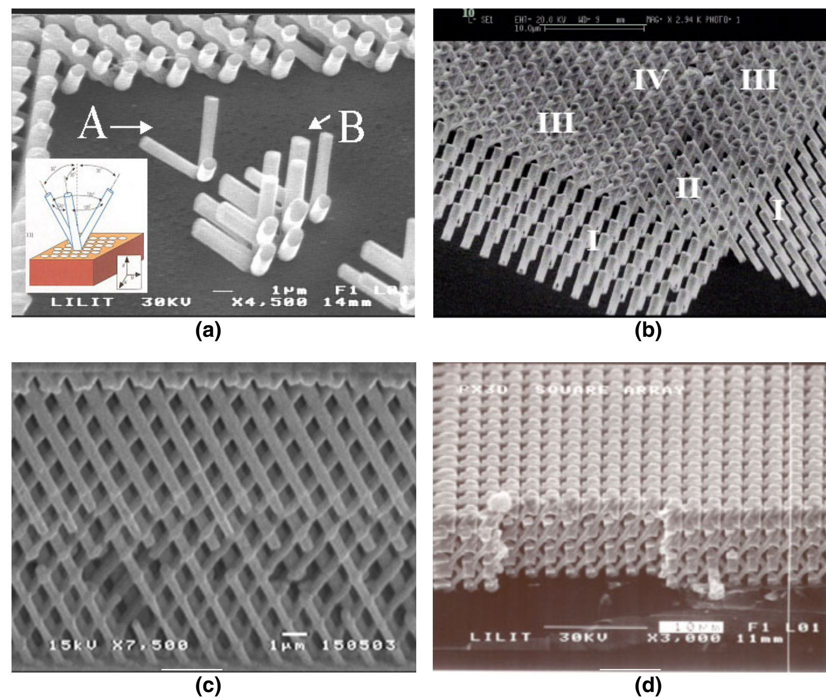

Figure 6. SEM micrographs illustrating various 3D PC lattices realized by multiple-tilted x-ray lithography. (a) A *Yablonovite* lattice generation scheme; inset structure A illustrates generation of a tripod-like structure by a single hole on the x-ray mask, and inset structure B exhibits *five crossing tripods* generated from five close holes on x-ray mask. (b) A 3D lattice structure fabricated by using four arrays of 45° tilted gold pillars along 90° crossing directions to generate a regular lattice. (c) Another *example of a 'Yablonovite'* lattice comprising crossing pillars generates up to 14 parallel lattice planes. (d) A complete fabricated nickel 3D PC lattice structure obtained by fourfold x-ray exposure of a square pattern array [28, 29].

A single hole generates a tetrahedral tripod-like structure (inset structure A in figure 6(a)). When the x-ray mask openings are close enough, the light paths are superposed and the holes intersect (inset structure B in figure 6(a); five tripods are generated from five holes on the x-ray mask, which in turn generates 15 pillars). When the x-ray mask openings were organized in a plane array and the exposure directions are along the major axis of the associated 3D lattice structure, then the exposed pillars organize themselves in a 3D lattice. In a similar manner, we realized various 3D PC lattices by multiple-tilted x-ray lithography and these are shown in figures 6(c) and (d). A tilted illumination of a symmetric array pattern generates an array of tilted pillars (region I in figure 6(b)). When another exposure is performed after an azimuth rotation of the mask + wafer around their normal axis, a second array of pillars is generated (see inset figure 6(a)). If the azimuth rotation is an angle of symmetry for the mask pattern, the second pillar array will intersect the first one at a set of 3D lattice points (see region II in figure 6(b)). Iterative repetition of the procedure over all the mask pattern symmetry directions will result in the generation of the full 3D lattice (region III and then IV in figure 6(b)). Thus, with a square symmetry array, four exposures in a 90° azimuth step will generate a cubic lattice. In contrast, the *Yablonovite* structure can be generated by threefold 120° step exposure of an equilateral triangle mask array (figure 6(b)). The vertical separation of the intersecting point planes will be determined by the tilt (zenith) angle. In the case of a cubic lattice the zenith

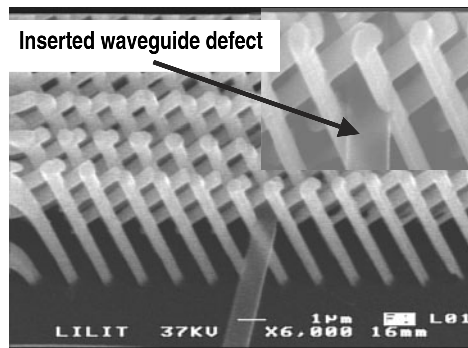

Figure 7. SEM micrographs showing a linear defect acting as a waveguide embedded in a 3D metallic photonic crystal (generated by the two-resist process). The inset in the picture details the waveguide.

angle is $\theta_c = 45°$. In the case of *Yablonovite* producing a unit cell with the form of a tetragon, the zenith angle becomes $\theta_Y = \arcsin 1/\sqrt{3} = 35.26°$. This method has been applied for the fabrication of nickel *Yablonovite* lattices with a lattice parameter of 1.3 μm and a total thickness of 15 μm, a value that allows us to achieve a full three-dimensional optical behaviour as confirmed by variable angle reflectance measurements. In figure 6(d), a complete 3D nickel lattice PC structure obtained by a fourfold multiple-tilted x-ray exposure is shown. The total structure thickness is 8 μm with a total of 14 completed layers parallel to the substrate. This is a remarkable number when compared to what was reported by Fleming *et al* [39], as for their cross stacked bar structure at least eight or nine layers are required to exhibit a PC behaviour.

The realization of 3D structures embedded with '*defects*' or waveguides has been accomplished by the newly developed and patented (pending) process based on the *two-resist process* [45] which is based on a *combined use of multiple-tilted x-ray lithography* [28, 29] *and e-beam lithography*. In this process scheme, two lithographic processes, namely multiple-tilted x-rays (as reviewed above) and electron beams, are performed on two resists, PMMA (low sensitivity) and SAL-607 ER (high sensitivity), which are characterized by chemically independent processes. The basic idea is to introduce linear defects at the interface by EBL between the two PMMA layers and perform around it a 3D lattice patterning by multiple-tilted XRL. This two-resist process approach allows the delineation of '*defect patterns*' by electron beam lithography on the top negative resist layer with *very low dose*, hardly affecting at all the bottom layer resist comprising low sensitivity PMMA resist. In principle, by electron beam lithography, *arbitrary shape patterns* or '*defects*' are being effectively defined in SAL-607 ER resist at the interface of PMMA layers. The process on the negative resist (SAL-607 ER), completed with post-baking and development, results in a chemically stabilized polymeric pattern of the designed '*defect*' or '*pattern*' lying on the top of the first PMMA layer. Once defect creation is accomplished, a second PMMA film is spun above the first one and a second x-ray exposure is performed. Finally, the whole PMMA multilayer has been developed simultaneously. The crucial characteristic that allows performance of x-ray lithography on the whole sample is that SAL is transparent to x-ray radiation but mechanically and chemically stable. The successive developing of the structure on the PMMA does not distort the defect patterning at the interface. The linear defects acting as *waveguides* were successfully embedded in a 3D metallic photonic crystal by the two-resist process as shown in figure 7, the inset in the picture detailing the waveguide. Further details, in regard to theory and experiments, are being reported elsewhere [44].

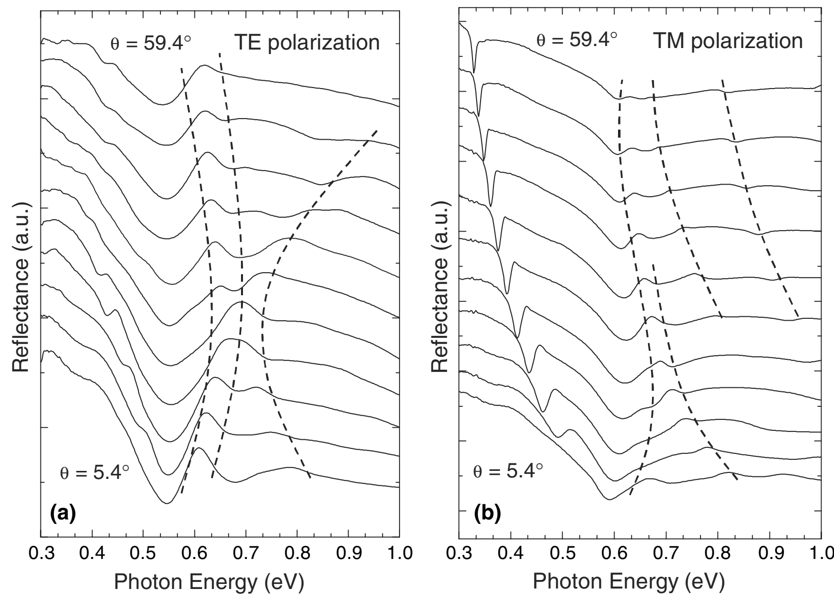

Figure 8. Variable angle reflectance of the sample shown in figure 6(d) for light incident along the G–X orientation, for TE (a) and TM (b) polarizations. The angle of incidence was varied from 5.4 to 59.4° with a steps of 5.4°. (The curves are vertically shifted for clarity [33].)

The preliminary optical characterization performed on the fabricated 3D nickel PC sample (figure 6(d)) is illustrated in figure 8. The experimental reflectance spectra showed several sharp features of well defined dispersions in their energy position as the angle of incidence was varied for TE (figure 8(a)) and TM polarizations (figure 8(b)). These observed resonances are very similar to those observed in 2D and 3D dielectric photonic crystals [18, 20, 43], and are presumably associated with the excitation of the 3D photonic bands of the metallic sample. The observation of such resonance structures is a clear demonstration of the very good quality and true three-dimensionality of samples. In particular, the sharp minimum observed at low energy in the TM reflectance spectra is attributable to the excitation of a *surface-plasmon polariton*, while the other steplike features are most probably associated with the excitation of the allowed *photonic modes* of the *metallic 3D structure*.

5. Magnetic material patterning and characterization

In the last decades patterned arrays of magnetic elements such as wires, dots and antidots have attracted a lot of interest both for their potential applications in magnetic data-storage devices and for the investigation of magnetic phenomena in low dimensional systems. Understanding and controlling their magnetization reversal and domain structure becomes a very important aspect in submicron magnetic systems, an interest motivated in part by applications to the magnetic recording industry. Periodic arrays of nano-magnets having dimensions of 100 nm or less can enhance the storage capacity with the added advantage of improved signal to noise ratio in data storage elements. However, the use of micro- and nano-structures in magnetic high density recording media and non-volatile random access memories is not trivial. If compared to the case of a continuous film, for instance, the finite lateral dimensions of the magnetic elements enhance the role of the demagnetizing field affecting both the static and

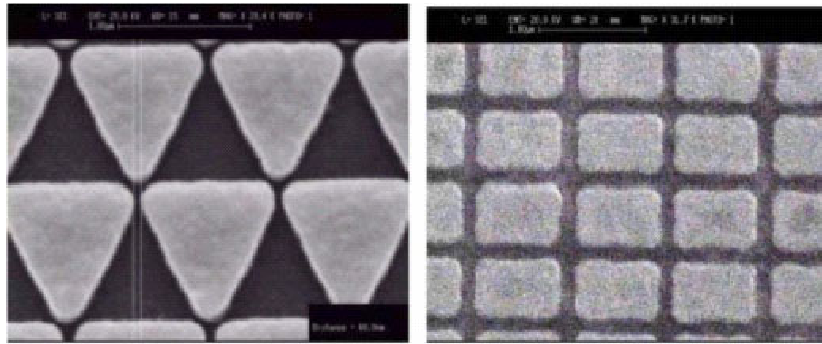

Figure 9. Nickel patterns fabricated by XRL. The Ni film is 35 nm thick, with pattern dimensions ranging from 250 nm to 1 μm.

the dynamical magnetic properties. Moreover, new effects due to the lateral confinement of the structures occur, such as the frequency quantization of spin-wave modes. Because of these fundamental and technological interests in nanoscale magnetic dot arrays, both the fabrication and the characterization of large uniform arrays of magnetic nano-structures are very important.

Nano-patterning and their characterization is another activity, in which we are using x-ray lithography [46, 47]. Use of x-ray lithography represents a clear advantage, because with this technique it is possible to replicate structures on a wide area with high resolution into thick resist films. We are using x-ray lithography to fabricate arrays of nano-magnets of period 100–200 nm. The particles are formed by electro-deposition, by evaporation and lift-off, or by etching of a previously deposited film. In figure 9, nickel perm-alloy patterns fabricated by XRL are shown. The Ni film is 35 nm thick, with pattern dimensions ranging from 250 nm to 1 μm. A detailed magnetic characterization of the dot arrays accomplished by magneto-optical Kerr effect give evidence for the effects of the shape anisotropy on the hysteresis loops which have also been verified by a micro-magnetic simulation. Furthermore, the BLS experiments clearly revealed the spin-wave quantization and the observed modes are identified as discrete, stationary surface spin waves.

6. Microfabrication using LIGA technology

A dedicated deep x-ray lithography (DXRL) beamline [3] with photon energy between 2 and 20 keV is operating at ELETTRA to produce high aspect ratio microstructures. A brief overview of some applications in the field of x-ray and visible optical components, micromechanical systems and microfluidic devices is presented here.

6.1. Novel x-ray optical elements

Masking devices for high energy x-rays are of great interest for synchrotron scientists. Deep x-ray lithography combined with metal electroplating allows the fabrication of thick Cu, Ni or Au metal sheets containing complex 2D hollow micropatterns. The ELETTRA pinhole array imaging system (PAIS) is a simple extension of a pinhole camera extension system [48]. Instead of a single pinhole the system integrates 50 equidistant pinholes of 50 μm diameter on a copper foil (figure 10(a)). The PAIS allows measurement of the main characteristics of the bending magnet radiation such as the source size, the vertical opening angle, the position of the source and the emission angle. The images detected by the CCD camera are also used to

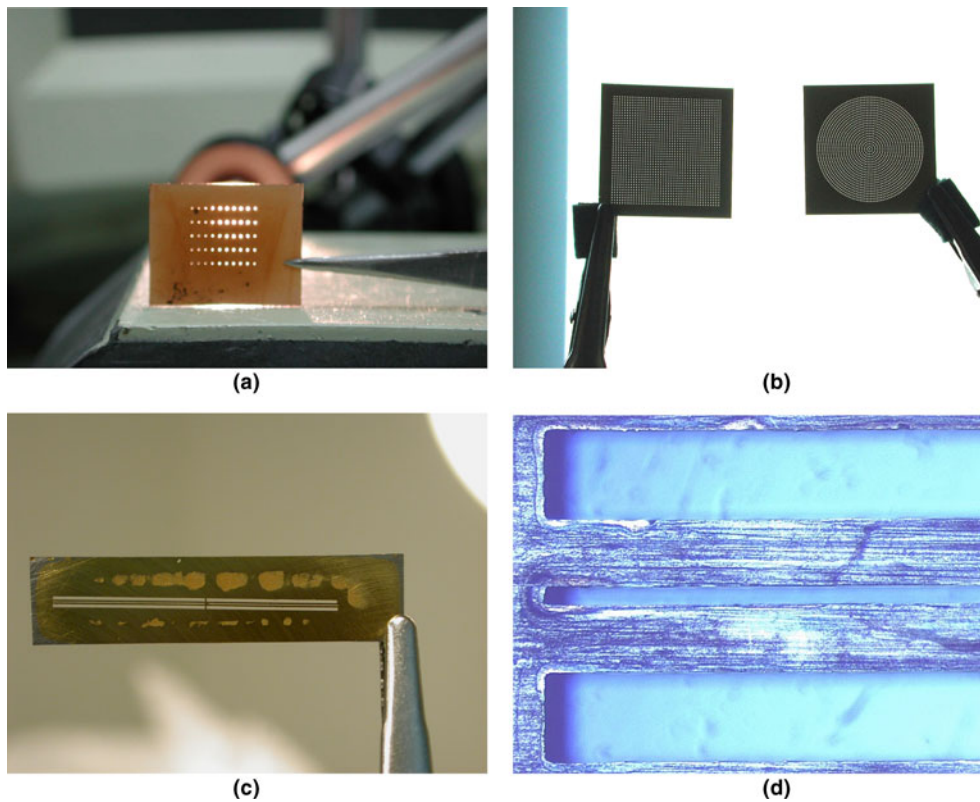

Figure 10. (a) Nickel mould inset obtained from the PMMA (DXRL) fabricated pyramid and (b) moulded identical pyramids in Zeonex.

monitor the transverse and longitudinal beam instabilities. A similar device was fabricated for x-ray photon correlation spectroscopy (XPCS) with a coherent beam at the Troika beamline of ESRF. A fast 2D gas detector has been developed, achieving good timing but not the appropriate spatial resolution. In order to improve the resolution two pinhole arrays were designed to be inserted in front of the detector. One is a 41×41 (figure 10(b) (left)) square array of equally spaced circular pinholes with 100 μm diameter. The other is a circular distributed array of 1681 pinholes (figure 10(b) (right)). A slit system (figures 10(c) and (d)) used in conjunction with a three-layer silicon microstrip detector prototype, available at the SYRMEP (Synchrotron Radiation for Medical Physics) beamline at ELETTRA was also fabricated. By means of this slit system, each detector layer is illuminated in a different fashion, allowing the acquisition of different kind of image (absorption, scattering, phase-contrast) in a single shot. Applications of the technique to medicine and biology are currently under investigation.

6.2. Pyramid wavefront sensors for telescope adaptive optic systems

Pyramid wavefront sensors are the key components of new multiconjugate adaptive optics systems used for wavefront correction of terrestrial telescopes [49]. The sensor consists of a very flat four-face pyramid made in a transparent material that requires an accurate control of the quality of its turned edges, its surfaces and the size of its pyramid tip. Moreover, identical copies of these optical elements are needed to fulfil the requirements of the multiconjugate

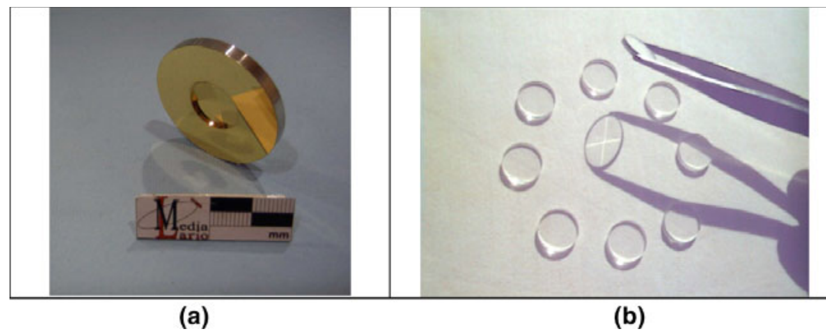

Figure 11. Cu electroplated micro-turbine rotors of 10 and 3.2 mm external diameters.

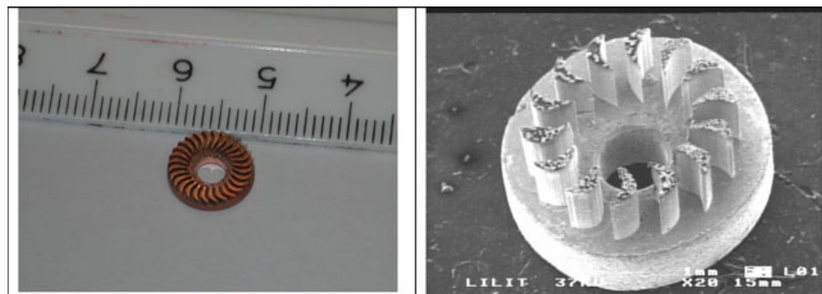

Figure 12. Fabricated microgear and array of hollow sharp tipped microneedles as part of the drug delivery system.

adaptive optics systems. A new fabrication method of pyramid wavefront sensors using the LIGA process was proposed to replace the classical glass figuring and polishing techniques that has been unable so far to provide a repeatable and time efficient means of fabrication. To fabricate the device [50], a PMMA cylinder whose axis is tilted towards the vertical direction of an angle α_i corresponding to the desired pyramid vertex angle is exposed to x-rays. A nickel blade with a super-polished edge was used as a mask to form the first face of the pyramid. The operation is repeated three more times, rotating the cylinder through 90° around its axis after each face exposure. After development the irradiated zones of the PMMA cylinder above the four faces are etched away in a GG developing bath, leaving a pyramid with a vertex angle of $\gamma = 180° - 2\alpha_i$ and a tip at the centre of the circular base. The repeatability of the manufacturing process is achieved using the PMMA pyramid as a template to fabricate a nickel mould, and thus produce several identical devices by moulding process [51]. Fabricated device is illustrated in figure 12.

6.3. Microturbine

The design and fabrication of a working prototype of a microturbine to generate electrical power from pressurized gas is underway for their potential application to meet on-board power requirements of micro-satellites (∼10 W). The deep x-ray lithography permits the manufacture of a turbine with high aspect ratio rotor blades (figure 11), allowing us to improve the overall power efficiency. Details of fabrication and characterization will be reported elsewhere.

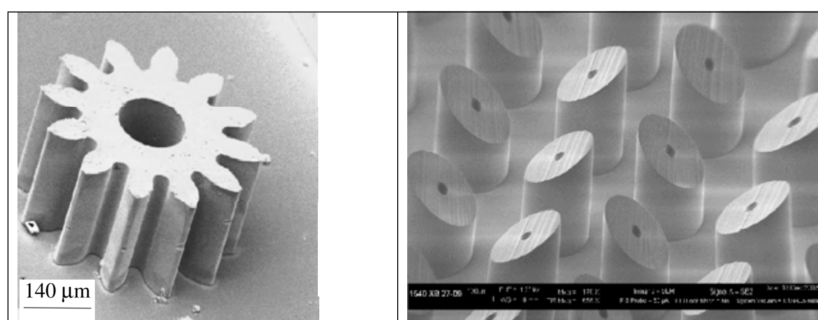

Figure 13. Fabricated micro-turbine rotor by LIGA process.

6.4. Micro-fluidics for drug delivery

The field of micro-fluidics is experiencing a rapid growth with applications for use in chemistry, microbiology and medicine. Typical examples in the medical field are implantable micro-devices capable of sensing biological parameters and delivering small and precise quantity of drugs into the body. Controlled transdermal drug delivery systems have the potential to seriously improve the treatment of certain disease as well as patient comfort. One can think of a portable device combining micro-fluidic elements and controlled electronically that would release drug molecules inside the body at programmable rates during a defined period. A study was started to design and fabricate a drug delivery system combining a LIGA fabricated micro-gear pump and micro-needle array (figure 13). The liquid containing the drug molecules is pumped from a reservoir by a gear pump and sent though a vertical aperture versus the micro-needle array painlessly clamped on the patient's skin. The output pressure of the gear pump must be sufficient to allow the liquid to flow through the tiny channels of the micro-needles. Accurate electrical control of the motor driving the gear pump allows very precise monitoring of the quantity of liquid that flows through the system without the need of a flowmeter. No valves are required, simplifying the design and fabrication process.

7. Conclusions

We have presented a brief review of our activities being carried at our facility LILIT at ELETTRA in micro- and nano-fabrication. Though we employ diverse patterning techniques which include E-beam, FIB and many emerging and non-conventional patterning techniques for our research work in many diverse areas, in reviewed activities we have selected only those topics in which we have invariably been using x-ray nanolithography. DOEs has been the most comprehensively researched area of our group and we have been exploring many new avenues where DOEs can be used as a viable optical element for shaping electromagnetic beams in wide range of the spectrum. We have been continuously developing a variety of DOEs for photonic applications (couplers and mode converters), x-rays and, for neutrons, spectroscopic applications. We have presented a brief review of our activities in ZPs for x-ray and neutron focusing and presented some new development in ZPs being under investigation. Photonics is another area of our research activities. However, again, we have restricted our review to the photonics bandgap crystal in which we have used our skill in x-ray nano-patterning for creation of novel 2D and 3D structures. Some of the other interesting activities in which we have been applying XRL, DXRL and LIGA techniques are also presented briefly.

Acknowledgments

This work was supported by the Italian ministry MIUR by a financial grant for the FIRB Project under No RBNE01XPYH.

References

[1] Di Fabrizio E, Nucara A, Gentilli M and Cingolani R 1999 *Rev. Sci. Instrum.* **70** 1605
[2] Filippo R, Di Fabrizio E, Vaccari L, Altissimo M, Cojoc D, Businaro L and Cabrini S 2001 *Microelectron. Eng.* **57/58** 101
[3] Pérennès F, De Bona F and Pantenburg F J 2001 *Nucl. Instrum. Methods* A **467/468** 1274
[4] Prasciolu M, Kumar R, Cabrini S, Businaro L, Cojoc D, Di Fabrizio E, Liberale C, Degiorgio V, Gigli G, Pisignano D and Cingolani R 2003 *Japan. J. Appl. Phys.* **42** 4177
[5] Schiappelli F, Kumar R, Prasciolu M, Cojoc D, Cabrini S, De Vittorio M, Visimberga G, Gerardino A, Degiorgio V and Di Fabrizio E 2004 *Microelectron. Eng.* **73–74** C 347
[6] Cojoc D, Di Fabrizio E, Businaro L, Cabrini S, Romanato R, Vaccari L and Altissimo M 2002 *Microelectron. Eng.* **61/62** 963
[7] Di Fabrizio E, Romanato F, Gentili M, Cabrini S, Kaulich B, Susini J and Barrett R 1999 *Nature* **401** 895
[8] Wilhein T, Kaulich B, Di Fabrizio E, Romanato R, Cabrini S and Susini J 2002 *Appl. Phys. Lett.* **78** 2082
[9] Soret J L 1852 *Arch. Sci. Phys. Nat.* **52** 320
[10] Sayre D, Howells M, Kirz J and Rarbeck H (ed) 1987 *X-Ray Microscopy II* (New York: Springer)
[11] Bionta R M, Ables E, Cook K J, Edwards O D, Gabriele P C, Jankowski A F, Makawiecki D M, Ott L L and Thomas N 1988 *SPIE* **984** 247
[12] Altissimo M, Romanato F, Vaccari L, Businaro L, Cojoc D, Kaulich B, Cabrini S and Di Fabrizio E 2002 *Microelectron. Eng.* **61/62** 173
[13] Kaulich B, Wilhein T, Di Fabrizio E, Romanato F, Altissimo M, Cabrini S, Fayard B and Susini J 2002 Differential interference contrast x-ray microscopy with twin zone plates' *J. Opt. Soc. Am.* A **19** 797
[14] Wilhein T, Kaulich B, Di Fabrizio E, Cabrini S, Romanato F and Susini J 2001 Differential interference contrast x-ray microscopy with sub-micron resolution *Appl. Phys. Lett.* **78** 2082
[15] Altissimo M, Petrillo C, Sacchettii F, Ott F and Di Fabrizio E 2004 *Microelectron. Eng.* **73–74** C 644
[16] Kearney P D, Klein A G, Opat G I and Gähler R 1980 *Nature* **287** 313
[17] Yablonovitch E, Gmitter T J and Leung K M 1991 *Phys. Rev. Lett.* **67** 2295
Yablonovitch E and Leung K M 1991 *Nature* **351** 278
[18] Romanato F *et al* 2002 *Nanotechnology* **13** 644
[19] Malvezzi A *et al* 2002 *J. Opt. Soc. Am.* B **19** 2122
[20] Galli M, Agio M, Andreani L C, Atzeni L, Bajoni D, Guizzetti G, Businaro L, Romanato F, Di Fabrizio E and Passaseo A 2002 *Eur. Phys. J.* B **27** 79
[21] Todaro M T, Stomeo T, Vitale V, De Vittorio M, Passaseo A, Cingolani R, Romanato F, Businaro L and Di Fabrizio E 2003 *Microelectron. Eng.* **67/68** 670
[22] Businaro L, Romanato F, Candeloro P, Di Fabrizio E, Patrini M, Galli M, Andreani C, Passaseo A and De Vittorio M 2003 *J. Vac. Sci. Technol.* B **21** 748
[23] Bennicia E, Ferreroa S, Giorgisa F, Pirria C F, Rizzolib R, Schina P, Businaro L and Di Fabrizio E 2003 *Physica* E **16** 539
[24] Malvezzi A M, Vecchi G, Patrini M, Guizzetti G, Andreani L C, Romanato F, Businaro L, Di Fabrizio E, Passaseo A and De Vittorio M 2002 *Phys. Rev.* B **68** 161306
[25] Andreani L C, Guizzetti G, Patrini M, Vecchi G, Malvezzi A M, Businaro L, Romanato F, Di Fabrizi E and Passase A 2003 *Phys. Status Solidi* B **238** 428
[26] Andreani L C *et al* 2002 *Physica* E **17** 402
[27] Patrini M, Galli M, Agio A, Andreani L C, Bajoni D, Guizzetti G, Businaro L, Di Fabrizio E, Romanato F and Passaseo A 2003 *Physica* E **17** 418
[28] Romanato F *et al* 2003 *Microelectron. Eng.* **67/68** 479
[29] Romanato F, Cojoc D, Di Fabrizio E, Galli M and Baioni D 2003 *J. Vac. Sci. Technol.* B **21** 2912
[30] Hector S D, Schattenburg M L, Anderson E H, Chu W, Wong V V and Smith H I 1992 *J. Vac. Sci. Technol.* B **10** 3164
[31] Guo J Z Y, Leonard Q, Cerrina F, Di Fabrizio E, Luciani L, Gentili M and Gerold D 1992 *J. Vac. Sci. Technol.* B **10** 3150
[32] Vos W L, Megens M, van Kats C M and Bosecke P 1996 *J. Phys.: Condens. Matter* **8** 9503

[33] Feiertag G *et al* 1997 *Appl. Phys. Lett.* **71** 1441
[34] Cuisin C, Chen Y, Decanini D, Chelnokov A, Carcenac F, Madouri A, Lourtioz J M and Launois H 1999 *J. Vac. Sci. Technol.* B **17** 3444
[35] Campbell M, Sharp D N, Harrison M T, Denning R G and Turberfield A J 2000 *Nature* **404** 53
[36] Vlasov Y A, Bo X-Z, Sturm J C and Norris D J 2001 *Nature* **414** 289
[37] Judith E, Wijnhoven G J and Vos W L 1998 *Science* **281** 802
[38] Shoji S and Kawata S 2000 *Appl. Phys. Lett.* **76** 2668
[39] Fleming G J, Lin Sy, Kady E I L, Biswas R and Ho K M 2002 *Nature* **417** 52
[40] Imhof A and Pine D J 1997 *Nature* **389** 948
[41] Holland B T, Blanford C F and Stein A 1998 *Science* **281** 538
[42] Kapitonov A M, Gaponenko N V, Bogomolov V N, Prokofiev A V, Samoilovich S M and Gaponenko S V 1998 *Phys. Status Solidi* a **165** 119
[43] Wijnhoven J E and Vos W L 1998 *Science* **281** 802
[44] Romanato F, Kumar R and Dr Fabrizio E 2004 *Nanotechnology* (communicated)
[45] Romanato F, Di Fabrizio E and Kumar R 2003 Process for the fabrication of sub-micrometric complex three dimensional structures by means of two resist combinated lithography *Patent No.* TO2003A000730 (filed on 23.09.2003)
[46] Candeloro P, Businaro L, DiFabrizio E, Conti M, Gubbiotti G, Carlotti G and Gerardino A 2002 *Elettra Res. Highlights* 35
[47] Candeloro P *et al* 2003 *Japan. J. Appl. Phys.* **42** 3802
[48] Galimberti A, Borghes R, Fava C, Gambitta A, Pérennès F, Pilosi M, Presacco R and Turchet A 2002 *Proc. EPAC 2002 Conf. (Paris, France, 2002)* pp 1891–3
[49] Ragazzoni R 1996 *J. Mod. Opt.* **43** 289
[50] Pérennès F, Ghigo M and Cabrini S 2003 *Microelectron. Eng.* **67/68** 566
[51] Pérennès F, Ghigo M, Tormen M and Cabrini S 2004 *Microsyst. Technol.* at press